



















## Article

# Radon Mitigation Applications at the Laboratorio Subterráneo de Canfranc (LSC)

Javier Pérez-Pérez <sup>1,\*</sup>, Julio Cesar Amare <sup>2</sup>, Iulian Catalin Bandac <sup>1</sup>, Alberto Bayo <sup>1</sup>, Silvia Borjabad-Sánchez <sup>1</sup>, Jose Maria Calvo-Mozota <sup>1,3,4</sup>, Laura Cid-Barrio <sup>1</sup>, Rebecca Hernández-Antolín <sup>1</sup>, Beatriz Hernández-Molinero <sup>1</sup>, Pau Novella <sup>5</sup>, Krzysztof Pelczar <sup>6</sup>, Carlos Peña-Garay <sup>1</sup>, Beatriz Romeo <sup>1,7</sup>, Alfonso Ortiz de Solórzano <sup>2</sup>, Michel Sorel <sup>5</sup>, Jordi Torrent <sup>7</sup>, Alberto Usón <sup>5</sup>, Anna Wojna-Pelczar <sup>6</sup> and Grzegorz Zuzel <sup>6</sup>

<sup>1</sup> Laboratorio Subterráneo de Canfranc (LSC), 22880 Canfranc-Estación, Spain; ibandac@lsc-canfranc.es (I.C.B.); abayo@lsc-canfranc.es (A.B.); sborjabad@lsc-canfranc.es (S.B.-S.); jmcavlo@lsc-canfranc.es (J.M.C.-M.); lcid@lsc-canfranc.es (L.C.-B.); rhernandez@lsc-canfranc.es (R.H.-A.); bhernandez@lsc-canfranc.es (B.H.-M.); cpenya@lsc-canfranc.es (C.P.-G.); beatrix.87@hotmail.es (B.R.)

<sup>2</sup> Centro de Astropartículas y Física de Altas Energías (CAPA), Universidad de Zaragoza, 50009 Zaragoza, Spain; amare@unizar.es (J.C.A.); alfortiz@unizar.es (A.O.d.S.)

<sup>3</sup> Escuela Superior de Ingeniería y Tecnología, Universidad Internacional de La Rioja, Avenida de la Paz, 137, 26006 Logroño (La Rioja), Spain

<sup>4</sup> Departamento de Ciencias, Universidad Pública de Navarra, Campus de Arrosadia, 31006 Pamplona, Spain

<sup>5</sup> Instituto de Física Corpuscular, Parc Científic de la Universitat de València, C/ Catedrático José Beltrán, 2, 46980 Paterna, Spain; pau.novella@ific.uv.es (P.N.); sorel@fnal.gov (M.S.); ausonandres@gmail.com (A.U.)

<sup>6</sup> M. Smoluchowski Institute of Physics, Jagiellonian University, ul. Łojasiewicza 11, 30-348 Kraków, Poland; krzysztof.pelczar@gmail.com (K.P.); anna.wojna.pelczar@gmail.com (A.W.-P.); grzegorz.zuzel@uj.edu.pl (G.Z.)

<sup>7</sup> Donostia International Physics Center (DIPC), Paseo Manuel Lardizabal, 4, 20018 Donostia-San Sebastián, Spain; jordi.torrent@udg.edu

\* Correspondence: javier.perez.perez@uj.edu.pl or jperez@lsc-canfranc.es (J.P.-P.)

† Current address: Affiliation 6.



**Citation:** Pérez-Pérez, J.; Amare, J.C.; Bandac, I.C.; Bayo, A.; Borjabad-Sánchez, S.; Calvo-Mozota, J.M.; Cid-Barrio, L.; Hernández-Antolín, R.; Hernández-Molinero, B.; Novella, P.; et al. Radon Mitigation Applications at the Laboratorio Subterráneo de Canfranc (LSC). *Universe* **2022**, *8*, 112. <https://doi.org/10.3390/universe8020112>

Academic Editor: Philippe Laurent

Received: 29 December 2021

Accepted: 5 February 2022

Published: 9 February 2022

**Publisher's Note:** MDPI stays neutral with regard to jurisdictional claims in published maps and institutional affiliations.

**Abstract:** The Laboratorio Subterráneo de Canfranc (LSC) is the Spanish national hub for low radioactivity techniques and the associated scientific and technological applications. The concentration of the airborne radon is a major component of the radioactive budget in the neighborhood of the detectors. The LSC hosts a Radon Abatement System, which delivers a radon suppressed air with  $1.1 \pm 0.2$  mBq/m<sup>3</sup> of <sup>222</sup>Rn. The radon content in the air is continuously monitored with an Electrostatic Radon Monitor. Measurements with the double beta decay demonstrators NEXT-NEW and CROSS and the gamma HPGe detectors show the important reduction of the radioactive background due to the purified air in the vicinity of the detectors. We also discuss the use of this facility in the LSC current program which includes NEXT-100, low background biology experiments and radiopure copper electroformation equipment placed in the radon-free clean room.

**Keywords:** radon; neutrinos; HPGe-detector; LSC



**Copyright:** © 2022 by the authors. Licensee MDPI, Basel, Switzerland. This article is an open access article distributed under the terms and conditions of the Creative Commons Attribution (CC BY) license (<https://creativecommons.org/licenses/by/4.0/>).

## 1. Introduction

Underground laboratories are the best places to explore science and develop technology in ultra-low radioactive background [1]. These laboratories have a rock shielding that blocks most of the cosmic rays, reducing the external background of the experiments several orders of magnitude. On the other hand, the surrounding rocks can have large concentrations of <sup>232</sup>Th, <sup>238</sup>U, and <sup>235</sup>U. These isotopes start the natural decay series that involve several radioisotopes and the emission of alpha, beta and gamma particles (see Figure 1) [2].

One of the elements of these decay chains is radon, a noble gas that can be emanated from the materials and increases laboratory air radioactivity due to its unstable isotopes.

(e.g.,  $^{222}\text{Rn}$  from  $^{238}\text{U}$ ,  $^{219}\text{Rn}$  from  $^{235}\text{U}$  and  $^{220}\text{Rn}$  from  $^{232}\text{Th}$ ). The most important radioactive background source among these radon isotopes is  $^{222}\text{Rn}$  from  $^{238}\text{U}$  chain, with the half-life of 3.82 days. This half-life is long enough to allow this radioactive isotope to escape from the material's surface, which increases significantly the overall radioactive background.

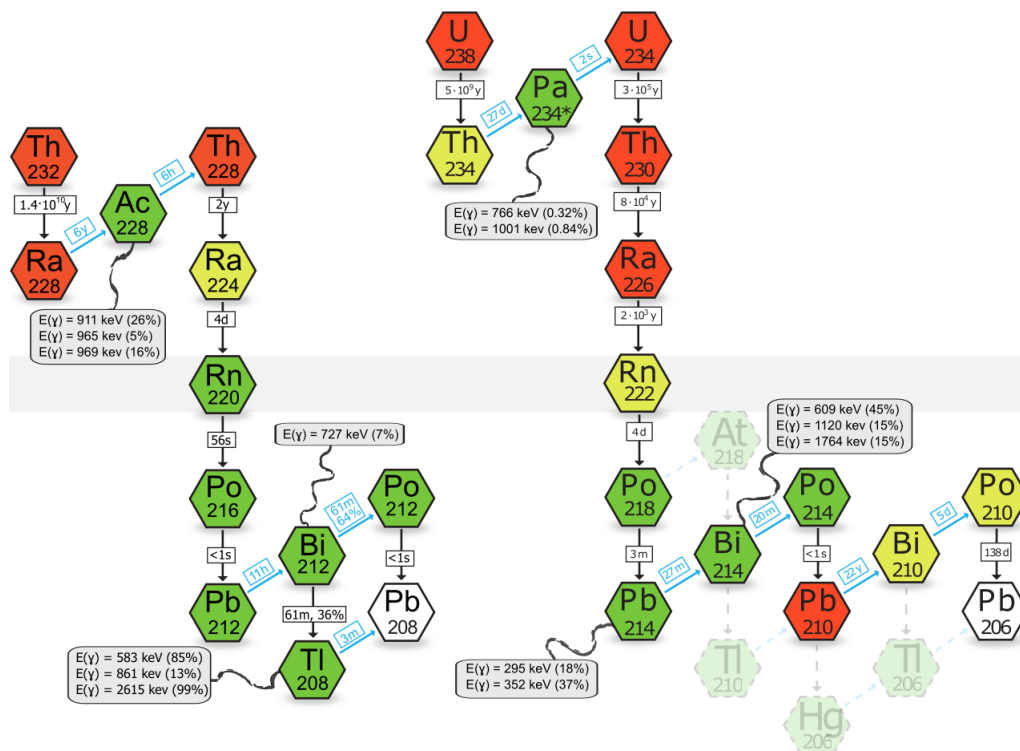


**Figure 1.** Radioactive chains. **Left:**  $^{232}\text{Th}$  decay chain; **Right:**  $^{238}\text{U}$  decay chain. In the grey boxes the most important gamma peaks energies and decay probabilities of the corresponding isotopes are presented.

In Figure 1 we used four different colours to identify isotopes: green for isotopes that decay fast (hours, seconds or shorter), yellow for intermediate decay time (days or months), red for long half-life isotopes (years) and white for the stable isotopes (the end of the different chains). When the secular equilibrium is broken, every isotope in red initiates a sub-chain in equilibrium. Light colored radioisotopes and arrows show low probability decay paths. Black downwards arrows represent alpha decays, while blue up-diagonal ones, beta decays. Half-lives of the isotope and decay probabilities of the branch are indicated next to the arrows. Finally, grey floating boxes contain the most relevant gamma energies emitted in the decays.

## 2. Laboratorio Subterráneo De Canfranc

Laboratorio Subterráneo de Canfranc (LSC) [3] is located in the Spanish side of the Pyrenees Mountains, under the Tobazo peak. It is situated between the international Somport road tunnel (that connects Spain and France) and the old train tunnel (not in use). The laboratory has a rock shielding of 800 m (Figure 2), equivalent to approximately 2400 meter water equivalent (mwe), that suppresses the cosmic muon flux by almost 5 orders of magnitude.

The total area of the underground laboratory is about 1600 m<sup>2</sup>, corresponding to a volume of about 10,000 m<sup>3</sup>. The laboratory is divided in four main areas: Hall A, Hall B, Hall C, Hall D and Hall E. Inside the laboratory several services are provided like a Clean Room (Class ISO 7/Class 10,000 and a Class ISO 6/Class 1000 in part of the room), an Ultralow Background Service (ULBS) using Gamma Spectrometry with High Purity

Germanium Detectors (HPGe) situated in Hall C, a mechanical workshop, the Radon Abatement System (RAS) and a liquid nitrogen production and distribution facility.

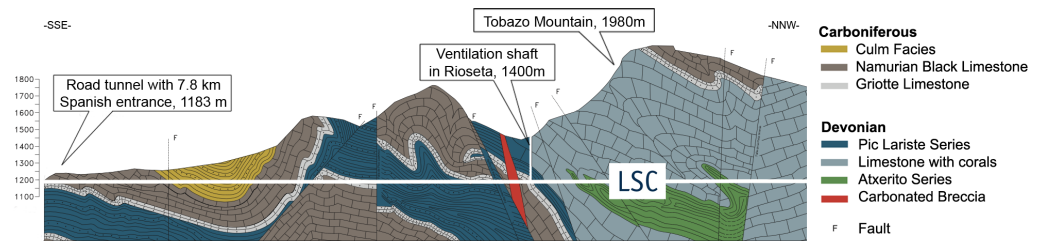


**Figure 2.** Laboratorio Subterráneo de Canfranc (LSC)—Longitudinal geological profile.

The fresh air inside the laboratory comes from the Rioseta air entrance, located on surface at 1400 m altitude. This air has to cross a 230 m vertical tunnel followed by a 700 m horizontal concrete tunnel excavated in the rock before being collected in a 100 m pipe that connects the tunnel and the laboratory. The air arrives to the Air Conditioning Room (Sala de Climatización, SC) of the laboratory and finally it is distributed in all the rooms of the laboratory with steel pipes, with a flow of 25,000 m<sup>3</sup>/h. This quantity plus the return air vent is enough to exchange all the air of the laboratory several times per hour.

The radon concentration in air is monitored with AlphaGuard detectors (AlphaGuard Saphimo P30 in Hall A, B and C; AlphaGuard Saphimo P2000 in Hall E). These detectors have a sensitivity of 1 CPM at 20 Bq/m<sup>3</sup>, a lower limit of  $\sim 2$  Bq/m<sup>3</sup>, and a calibration error of  $\pm 3\%$ . The average annual activity in the underground lab common area is  $(69.0 \pm 0.3)$  Bq/m<sup>3</sup> with daily, seasonal and annual fluctuations (see Figure 3 for Rn measurements performed in Hall A). The values obtained in different experimental halls inside LSC performed at the same time are compatibles [4]. The radon emanation depends on several external factors including rain or snow melting because water increases radon diffusion from the material surfaces and its later emanation [2,5–8].

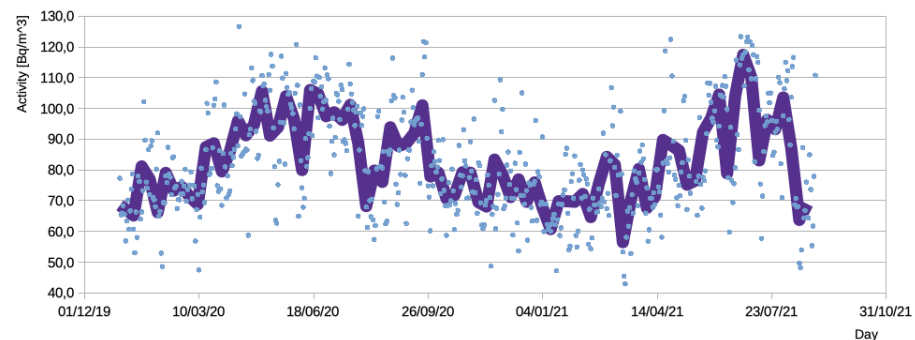


**Figure 3.** Radon measurements inside Hall A. Light blue points show the daily measurements and the violet line shows the weekly mean value.

A dedicated campaign of measurements was performed in the underground lab to identify the spatial distribution of the radon sources [9]. An AlphaGuard P30 detector was placed in several locations between the air entrance at Rioseta and the pipe that collects this air and guide it towards the Air Conditioning Room situated inside the underground laboratory. We observed an increase in the radon activity from about 20 Bq/m<sup>3</sup> at the entrance on surface (Rioseta) to approximately  $\sim 70$  Bq/m<sup>3</sup> at the entrance of the air inside the laboratory. This increase is caused by the radon emanated by the concrete of the two tunnels from the Rioseta entrance to the laboratory.

### 3. Radon Abatement System

The Radon Abatement System at LSC is a system that can provide very low radon-concentration air, of about  $\sim 1$  mBq/m<sup>3</sup>, with a flow from 180 to 220 m<sup>3</sup>/h. For many

applications, such level of radioactivity makes this air radon-free (Rn-free) in practice. The daily consumption of both  $N_2$  and  $LN_2$  (Liquid Nitrogen) is larger than what LSC can produce. The RAS is used to create large Rn-free spaces that are safe for people to work. The Rn-free air is cheaper and also reduces the dependence from external  $LN_2$  suppliers.

The RAS machine was built by the company Apparatuses Technologies Construction (ATEKO a.s.) from Czech Republic. For this reason, the radon-free air is also named ATEKO-air [10].

Other underground laboratories have similar facilities to reduce the radon activity [11,12]. For example, there are several installations made by ATEKO—Table 1 [13].

**Table 1.** ATEKO s.a. installations in Underground Laboratories.

Underground Lab.	Country	Average Rn ( $Bq/m^3$ )	Year	Air Flow [ $m^3/h$ ]
Modane	France	15	2004	150
Gran Sasso	Italy	80	2011	150
Gran Sasso	Italy	80	2012	220
Yangyang	Korea	40	2015	120
LSC	Spain	70	2015	220
SURF	USA	310	2017	300
Jin Ping	China	40	2019	300

The RAS takes the ambient air and compresses it to 10 bar. Then, the air is dried, filtered and sent to the cooling unit, where the air is cooled to a temperature of  $-60\text{ }^\circ\text{C}$ . In the next step, the air is moved to two adsorption columns with  $1\text{ m}^3$  volume each, where active carbon captures the radon atoms. Finally, the air temperature is adjusted to be heated back to room temperature and filtered again. For a schematic view of the RAS system, see Figure 4.

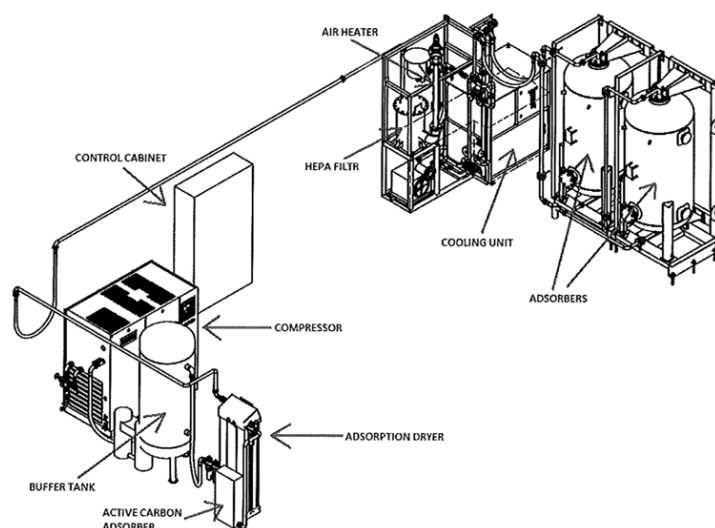


**Figure 4.** Scheme of the distribution of the elements of the RAS at LSC.

At the LSC, there are two different types of piping for the ATEKO-air: a pressurized Rn-free air line (7 bar) with several outlets at the Underground Laboratory, and an atmospheric pressure line used by the NEXT experiment, with over-pressures from 0 Pa to 5000 Pa (50 mbar). The RAS has been delivering continuously Rn-free air during the last 4 years, with a downtime of 0.2% due to maintenance.

#### 4. Electrostatic Radon Monitor

The Electrostatic Radon Monitor (ERM) [10] is a low background electrostatic detector that can measure in real time activities  $<1\text{ mBq}/m^3$  of  $^{222}\text{Rn}$  in the air using a Silicon  $\alpha$ -

particle Detector from Canberra model PIPS 1200-35-100AM as alpha detector. To evaluate the performance of the ATEKO-air, this air is continuously flowing through the ERM with a slight overpressure of 0.3 barg. Its scheme and a real picture of the top flange is shown in Figure 5. On the right side of the figure, the simulation of the electric field in the detector vessel is shown. The field is created by applying a high voltage (several kV) to the vessel while the alpha detector (black disc in the neck) installed on a top flange is connected to the ground potential. With the simulation, we estimate that  $\sim 90\%$  of the field lines cross the detector surface.

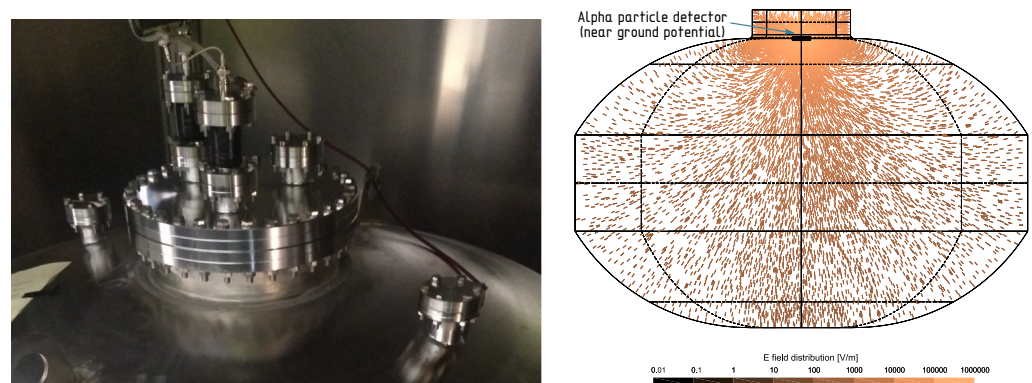


**Figure 5.** Left: Picture of the ERM. Right: Simulation of the electric field lines inside the ERM detector.

The detection efficiency has two contributions: charge collection efficiency and alpha detector efficiency. The charge collection is the process where the  $^{218}\text{Po}$  ions, produced after a  $^{222}\text{Rn}$  decay, are drifted to the alpha detector and collected. The average charge collection efficiency estimated by a detailed simulation of the vessel geometry with a volumetric efficiency of  $\sim 90\%$ . Some dead volumes (e.g., above the alpha particle detector) contribute to the remaining 10% of the volume (see [10] for more details). The intrinsic detection efficiency of the alpha detector is close to  $\sim 50\%$  as the decays occur right at the detector's surface (0 distance). It is actually less than that due to the edge effects (like the detector rim etc.). To measure the detection efficiency, a calibration with a  $^{222}\text{Rn}$  source was performed. The detection efficiency of the ERM is  $(30 \pm 4)\%$  for the  $^{218}\text{Po}$  and  $^{214}\text{Po}$   $\alpha$ -peaks at the operational voltage of 8 kV (see Figure 6, left). The detection efficiency is similar in all the peaks of both Polonium isotopes (we tend to refer to peaks—lines—in the energy spectrum having in mind the detection efficiency for particular Po decays). The quoted value refers to  $^{214}\text{Po}$ , which is less sensitive to gas contamination.

To estimate the background of the detector, we closed the flow of ATEKO-air during 1 month to reach the saturation regime—when the measured Rn concentration is actually the activity of emanated Rn (see Figure 6, right). This happens when the detector is sealed (no gas is flushed), and the emanated Rn activity has enough time to build up (saturate) to equilibrium between emanation and decay. The activity of the radon emanated from the detector in saturation is  $(3.0 \pm 0.5)$  mBq, which results in a small contribution (about 10% of the saturation value) during normal operation. The estimated detection limit of the detector is  $0.7$  mBq/m<sup>3</sup>.

A gas panel was designed to permit the operation of the ERM detector in various configurations (Figure 7 shows the scheme of the detector and the gas panel). There are three different gas inlets: one for N<sub>2</sub>, one for the ATEKO-air directly from the RAS and the other one for different uses. Currently, the detector is configured to input the ATEKO-air that comes back from NEXT after flushing inside the lead castle, around the detector. A built-in  $^{226}\text{Ra}$  calibration source (that emits  $^{222}\text{Rn}$ ) is connected to the gas panel. A gas pump is used to force circulation of the air through the detector.

To see if there is a dependency of the residual Rn in the ATEKO air on the Rn concentration outside the detector (input air), a study was made (In Figure 8) by comparing the daily activity measured with the AlphaGuards (normal air) and the daily activity measured with

the ERM (ATEKO-air). The AlphaGuard detector performs a measurement every 10 min, daily mean values were considered. In the case of ERM, some measurements are several days long; in this case we considered the corresponding mean value. The colored areas around the lines include the 1-sigma error. No clear correlation was observed between the Rn content in the ATEKO line and in the laboratory air. For this reason, it is mandatory to have dedicated detectors—ERM and AlphaGuard, to monitor the activity of the ATEKO-air and the external background, respectively.

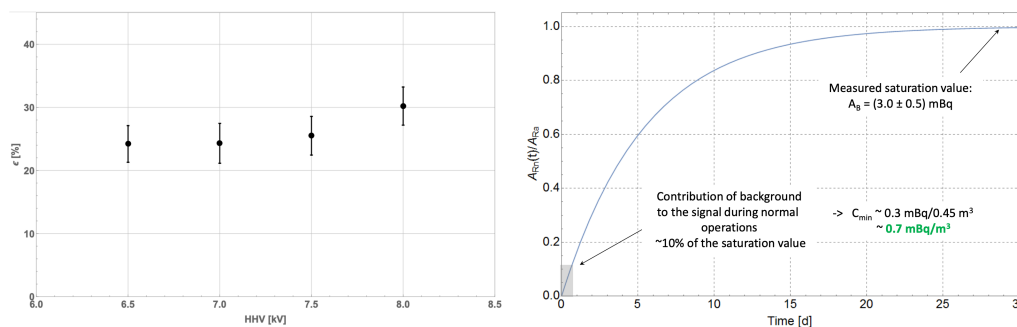


**Figure 6.** Left: Overall measured detection efficiency of the ERM for the  $^{218}\text{Po}$  and  $^{214}\text{Po}$  peaks as function of the operational voltage, HHV (High High Voltage). Right: The activity of radon emanated from the ERM detector (in saturation).

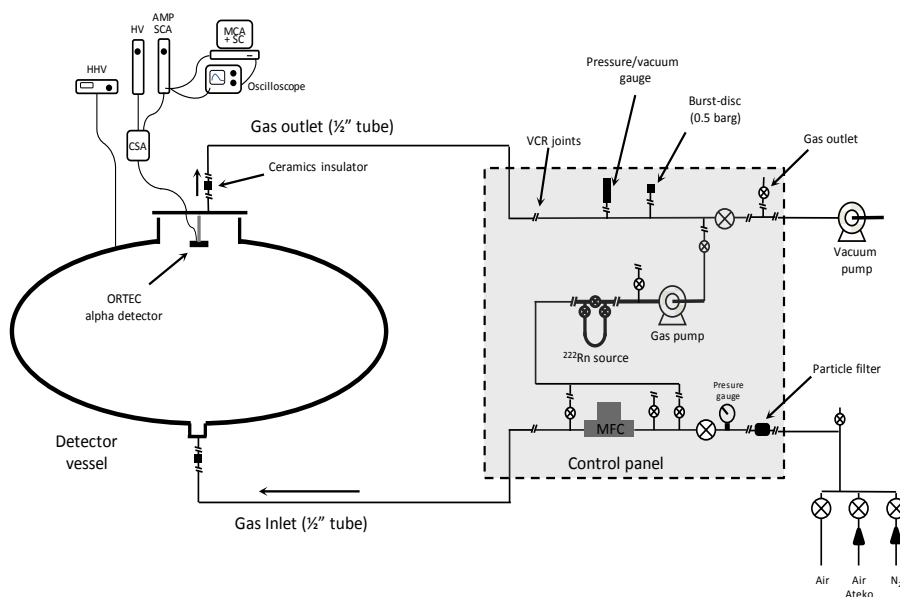


**Figure 7.** Schematic of the ERM detector and gas panel.

The ATEKO-air is very stable in time, demonstrated by calculating the mean value of the activities for the first half of 2020 and 2021. The mean activity was  $1.1 \pm 0.2 \text{ mBq}/\text{m}^3$ , in 2020 and also in 2021. It shows that the performance of the active carbon is good for long time usage. For this measurements the outlet flow from the ATEKO system was  $185 \text{ m}^3/\text{h}$ . We also evaluated how much Rn activity varies with the air flow selected in the ATEKO machine. From 8 June to 15 June 2020, the flow of the ATEKO-air was increased to maximum capacity, that is  $220 \text{ m}^3/\text{h}$ , with a mean activity of  $1.0 \pm 0.2 \text{ mBq}/\text{m}^3$  statistically compatible with the usual mean activity. This measurement was long enough to demonstrate no significant differences in activity between flows. The energy consumption required to generate a unit of flux (about  $1 \text{ Nm}^3/\text{h}$ ) of ATEKO-air depends on the outlet flux level produced by the system (see Figure 9). Therefore, activity is not an important factor to select the flow of Rn-free air.

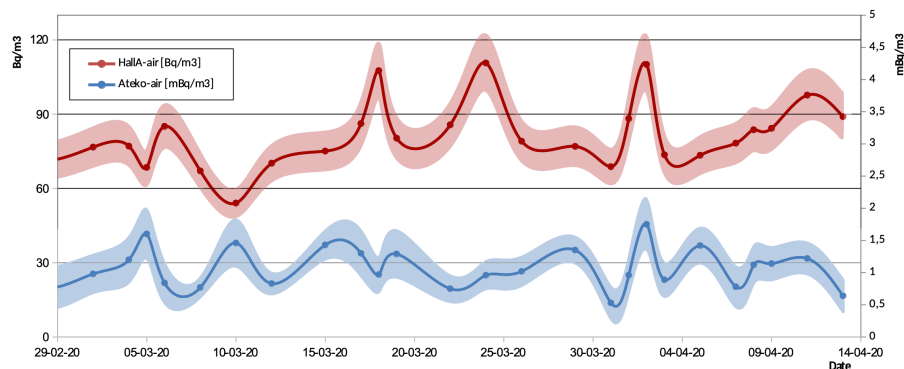


**Figure 8.** Comparison of radon activities vs time. We show the radon activity in Hall-A measured with an AlphaGuard (in red) in units shown in the left side *y*-axis and with the ERM (in blue) in units shown in the right side *y*-axis.

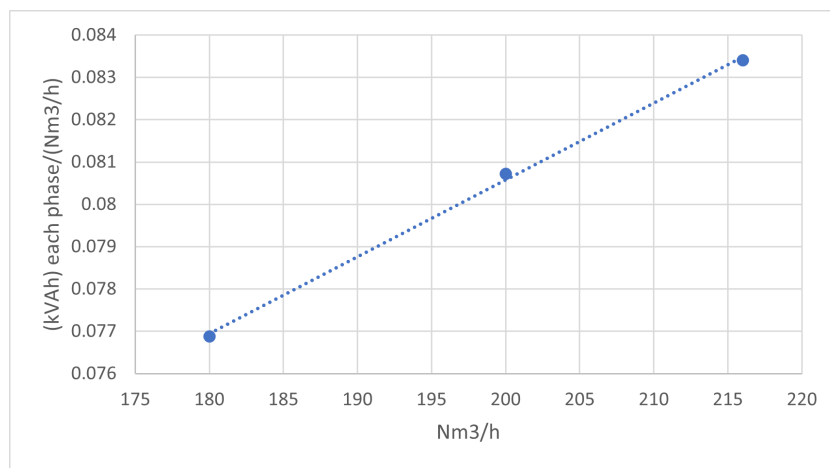


**Figure 9.** Energy consumption required to generate a unit of flux (about 1 Nm<sup>3</sup>/h) of ATEKO-air depends on the outlet flux level produced by the system.

### 5. ATEKO-Air to NEXT

The first experiment benefiting from the ATEKO-air in the underground lab was NEXT (Neutrino Experiment with a Xenon TPC) experiment [14]. NEXT collaboration is trying to identify the nature of neutrino, whether it is a Majorana fermion or not, with the observation of  $0\nu\beta\beta$  (Neutrinoless Double-Beta Decay) of <sup>136</sup>Xe, with  $Q_{\beta\beta} = 2.5$  MeV. The detector is a time projection chamber filled with xenon gas at pressure (7–15 bar), and two separated detection planes: the energy plane—which is used to measure the energy of events with PhotoMultiplier Tubes (PMT) with energy resolution (ER) <1%, and the tracking plane—which is used to track the electrons in the gas with Silicon photomultipliers (SiPM). The main sources of background to this experiment are the decays of two isotopes: <sup>214</sup>Bi (2.447 MeV, intensity: 1.57%) and <sup>208</sup>Tl (2.614 MeV, intensity: 100%)—as shown in Figure 1, with gammas very close to  $Q_{\beta\beta}$ .

An external Lead Castle (with 200 mm thickness) was built to shield the detector from the radioactive gamma background of the laboratory [15]. At the same time, a system to flush with ATEKO-air was developed. Inside the Castle a diffusor with 8 air outputs (each one with 8 horizontal holes and 1 vertical) was mounted to flush the detector with ATEKO-air (see below).

#### 5.1. Firsts Tests of the Castle

In 2014, before the RAS and the installation of NEXT-White detector and the diffusor, the initial plan was to reduce the Radon background inside the Castle by building it as air-tight as possible and flowing a small volume of N<sub>2</sub> inside. To evaluate this design,

several tests (from 29 October 2014 to 12 February 2015) [16] were done with a high pressure N<sub>2</sub> bottle, changing the flow and purging between measurements. These tests were made with the Castle completely built, with all the joints in place but before placing the vessel of NEXT-White on the pedestal. Therefore, the empty holes for the pipes of the Castle were covered with High Density Polyethylene (PE-500).

Two different detectors were placed inside the Castle for these measurements: one was an AlphaGuard Saphimo P2000 and the other was a 3" × 3" NaI(Tl) detector. The NaI(Tl) instrumented crystal is a low background detector that was connected to a Canberra 2005 preamplifier, a Tennelec linear amplifier and a Canberra 8701 ADC, and finally read by an Arduino board. The rate measured with the NaI(Tl) detector is shown in Figure 10. During these days, the Rn activity in Hall A was in the range of 60–80 Bq/m<sup>3</sup>.

To evaluate the contribution of the Castle, different setups were prepared:

1. Castle open. This measurement was taken before closing the Castle to have a reference value of the event rate. With the Castle open, the space between both sides of the Castle is 2.9 m, therefore it was only partially shielded from the gamma background coming from the laboratory. This measurement is not shown in Figure 10.
2. Castle closed, drawn in blue in Figure 10. Measurement done after closing the Castle.
3. Better closed Castle, drawn in red. Measurement done after improving the airtightness with additional joints, blocking the holes, etc.
4. After N<sub>2</sub> purge, drawn in yellow. A purge was done with N<sub>2</sub> with a flow of 1800 L/h for 7 h to remove the Rn inside the Castle.
5. N<sub>2</sub> purge + flux 180 L/h, drawn in green. A second purge was made but, after this, a constant flux of 180 L/h was injected into the Castle.
6. Without N<sub>2</sub> flux, drawn in violet. Measurement done after stopping the constant flow of N<sub>2</sub> in setup 5.
7. N<sub>2</sub> purge + flux 900 L/h, drawn in brown. Same conditions as in setup 5 but with a larger flux of 900 L/h.
8. Without N<sub>2</sub> flux, drawn in turquoise. Same as in setup 6, measurement made after stopping the N<sub>2</sub> flux.

The results of these measurements are presented in Figure 10 and Table 2. In the Figure, NaI(Tl) total rate as function of time for different tests (in different colors) are presented. In the third column of the table the average rate for each test is calculated. In the fourth column the Radon activity measured in short time windows for each test is shown.

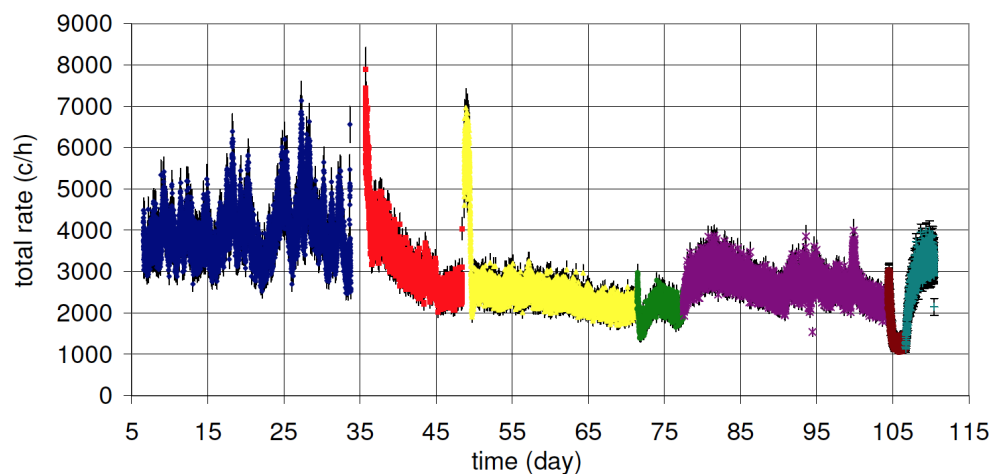


**Figure 10.** NaI(Tl) total rate as a function of time for different tests: **blue**—Castle closed; **red**—Castle closed with improved tightness; **yellow**—Castle closed with 7 h N<sub>2</sub> purge at 1800 L/h; **green**—Castle closed with N<sub>2</sub> purge + constant N<sub>2</sub> flux 180 L/h; **violet**—Castle closed without N<sub>2</sub> flux; **brown**—Castle closed with N<sub>2</sub> purge + N<sub>2</sub> flux 900 L/h; **turquoise**—Castle closed without N<sub>2</sub> flux.



**Table 2.** Measurements of the contribution of the NEXT Castle in different tests.

	Setup	Rate with NaI (Hz)	Activity with AlphaGuard (Bq/m <sup>3</sup> ) *
1	Castle open	59.56 ± 0.01	79 ± 28
2	Closed Castle	1.089 ± 0.001	79 ± 28
3	Better closed Castle	0.694 ± 0.002	30 ± 11
4	After N <sub>2</sub> purge	0.658 ± 0.001	30 ± 12
5	N <sub>2</sub> purge + flux 180 l/h	0.600 ± 0.001	22 ± 9
6	Without N <sub>2</sub> flux	0.638 ± 0.001	26 ± 10
7	N <sub>2</sub> purge + flux 900 l/h	0.350 ± 0.002	4 ± 3
8	Without N <sub>2</sub> flux	0.894 ± 0.002	47 ± 15

\* The AlphaGuard measurements were very short, only to obtain the order of magnitude.

In setup 7, we observe a large background reduction. But for this measurement the AlphaGuard detector is at its limit of sensitivity and the NaI(Tl) could be contaminated by gammas from other sources. Therefore, the use of Radon-free gas and more precise detectors are needed to improve the measurement.

## 5.2. Connection of NEXT to RAS

After the installation of the RAS and the ERM, the possibility of a cheaper and Rn-free air produced at LSC was the best option. Rn-free air is produced at LSC and can be precisely measured with ERM. Additionally, more flexible safety protocols around the Castle can be followed because there is no risk of suffocation. The connection between the RAS and NEXT can be divided into three different sections: Part I—LSC pipes system, Part II—the NEXT pipes outside the Castle, and Part III—the NEXT pipes inside the Castle.

### 5.2.1. Description of Part I—The LSC Pipe System

NEXT experiment and the RAS are in opposite parts of the Hall A, separated by about 60 m. Therefore, a pipe crossing the Hall A is used to deliver the air. The installation is made of AISI-316 Stainless Steel pipe with  $d = 4''$  (101.6 mm), welded, minimizing the number of joints. The length of this pipe is 59 m. All joints are using flat flanges, according to norm EN-1092-1 Type 1 PN-2.5. These flanges use rubber elastomeric gaskets. For the air distribution, two manual ball valves are mounted at the outlet of the RAS. In parallel to this installation, there is a pipe to return the air from NEXT Castle to the ERM with  $d = 1''$  (25.4 mm) and made of AISI-316 Stainless Steel, completely welded. This pipe has a length of 59 m and has unions with threaded fittings, according to norm DIN-2999.

### 5.2.2. Description of Part II—The NEXT Experiment Pipe System

The system consists of a pipe with diameter  $d = 1'' 1/2$  (38.1 mm) of AISI-316 Stainless Steel and several flexible pipes with  $d = 40$  or  $50$  mm of PVC (SPRINGVIN IBERFLEX). Pressed joints and threaded joints (type Pressfitting, INOXPRESS) are used to connect these pipes (see Figure 11). All these joints are using elastomeric gaskets of EPDM. For air distribution, several ball valves are employed. We used flexible pipes to allow the opening of the external Lead Castle and best suited to seismic vibrations affecting the installation.

The NEXT pipe system includes several gauges:

1. A flow meter Pro dual IVL10N with two output signals (for ventilation and air conditioning). The signals correspond to air flow velocity and temperature inside the air duct.
2. A differential pressure sensor WIKA Model A2G-50 (for ventilation and air conditioning). This sensor measures the air pressure at three different points of the installation using solenoid valves:
  - (a) the pressure in the Rn-free air inlet line,
  - (b) the pressure in the pipe entering in the NEXT Castle and,
  - (c) the pressure inside the Castle, around the detector.
3. A manual flow-control valve to control the air flow to the Castle.

4. Several manual ball valves located in different 'bypasses', installed for tests purposes for the RAS and the ERM.
5. The system is monitored by an Arduino ARDBOX 20, from Industrial Shields.

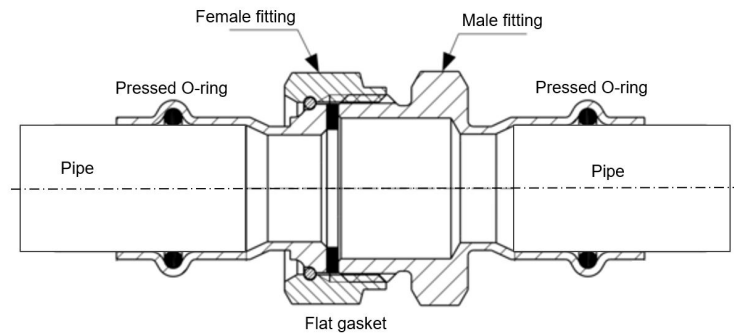


**Figure 11.** Lateral section of the pressed joints and threaded joints, pressfitting INOXPRES.

### 5.2.3. Description of Part III—The Diffusor, the Detector and the Castle

The air diffusor is placed inside the Castle, above the NEXT detector. This diffusor is designed to homogeneously distribute the ATEKO-air inside the Castle and displace the normal air (see Figure 12). In this Figure, the air flow injected by the diffusor is shown in light blue. This diffusor is designed to be used for both NEXT-White and NEXT100 detectors.

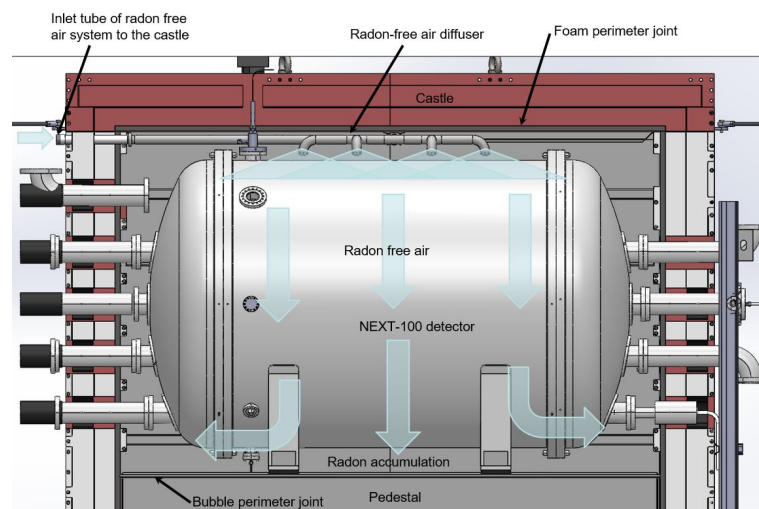


**Figure 12.** Side view of the Rn-free air diffusor, the Castle and the NEXT100 detector.

We show an upper cut (without the roof of the Castle) of the diffusor and the NEXT-100 vessel in Figure 13. The flows of injected air from the 8 tubes of the diffusor were marked with blue circles, above the detector. The Castle (in red) is divided into two mobile parts. Both sides are independent and can be moved to get access to the detector. For this purpose, a system with rails, wagon wheels, and two electric motors to open and close the Castle was implemented.

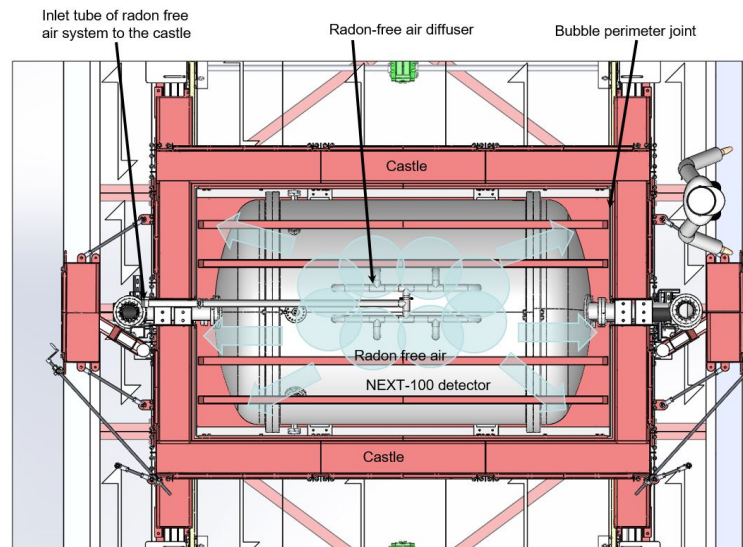


**Figure 13.** Top view of the closed Castle with a scheme of the distribution of the Rn-free air.

The Castle is shown with the right side opened in Figure 14, where five of the ten pipes coming from the RAS can be seen. The ten pipes (DN-100) are crossing the two mobile parts of the lead of the Castle. To improve the Castle airtightness and reduce the gamma background around the detector, special lead bricks were machined to perfectly seal the space around the pipes. With these bricks in place, the Castle can be opened and closed without manually removing any other part of the shielding. There are foam fillings in all the joints between the two mobile sides of the Castle and there is a bubble joint in the union between the pedestal and the two mobile parts. All these joints are necessary to keep the Castle air-tight.

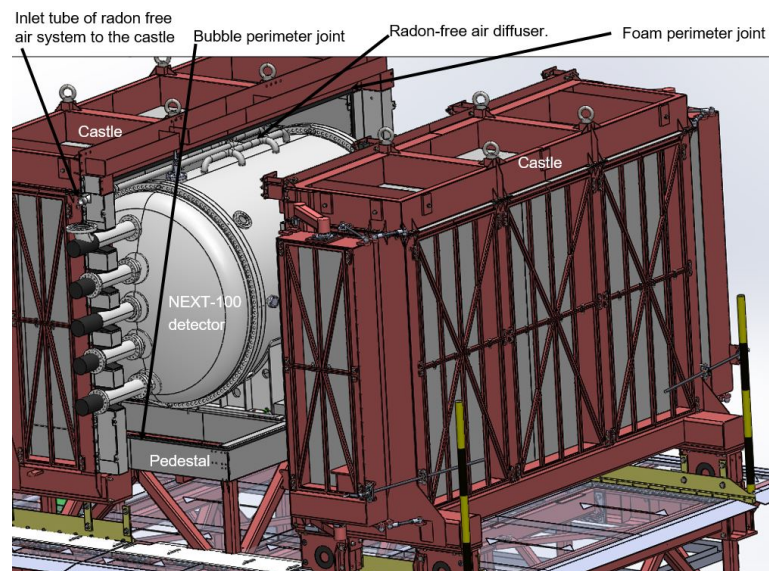


**Figure 14.** NEXT detector. Details of the connection system with the ATEKO machine.

A closer view on a diffuser is shown in Figure 15. It has 8 perimetral holes and 1 central, all of them of diameter  $d = 5$  mm. Radon tends to accumulate above the pedestal. For this reason, these diffuser tubes are designed to displace it using a large ATEKO-air flow injection. The air will escape from the Castle through the external perimeter of the pedestal and also through the small holes between the pipes and the lead (small leaks).

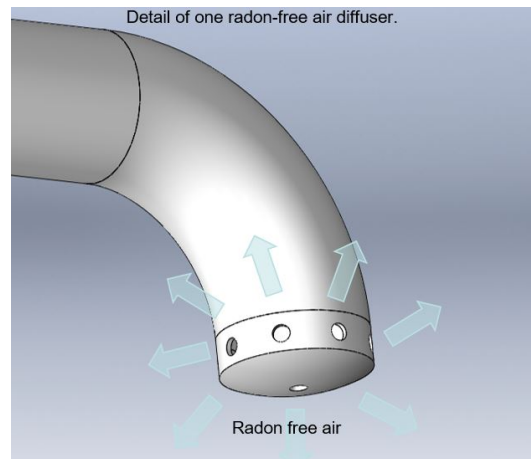


**Figure 15.** Diffuser detail: 8 perimetral holes and 1 central, all of them of diameter  $d = 5$  mm.

### 5.3. Tests of the Pipes and the Castle

Due to the large distance between the RAS and the ERM, long pipes were needed: pipes from the LSC setup are 59 m long and the ones from setup NEXT are 8 m long. Considering also the return line, the total distance is 134 m. To evaluate as precisely as possible the radon contribution of the different parts of the system, 3 different tests were performed (see Figure 16 and Table 3). It is important to evaluate the contribution of all parts because some pressed tubes were used instead of welded stainless steel pipes. Pressed tubes are cheaper and easier to mount.

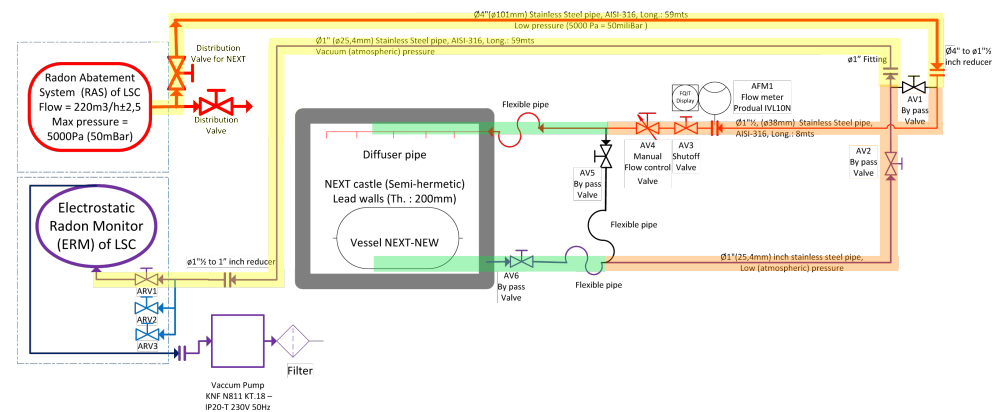


**Figure 16.** Paths used for the three different measurements of Rn activity

**Test-1** (Part I—path marked in yellow in Figure 16) takes the ATEKO-air and crosses all the Hall A and returns to the ERM to measure the Rn activity of the air. To isolate this circuit, AV1 bypass valve was used. The total length of this circuit is 118 m.

**Test-2** (Part I and Part II—paths marked in yellow and orange in Figure 16) includes all pipes but not entering inside the Castle. In this case, AV1 was closed and AV5 opened. The total length of this circuit is 132 m.

**Test-3** (Part I, Part II and Part III—paths marked in yellow, orange and green in Figure 16) uses the final setup used in NEXT. The ATEKO-air enters the Castle and, through the diffusers, bathes NEXT-White detector. To complete the circuit, a small open pipe at the base of the pedestal takes the air into the return line. The open pipe is placed where the Rn accumulates with the air flowing (lower part of the Castle). With this setup, there is no overpressure so we use a pump to force the circulation of the air towards the ERM. AV1 and AV5 are closed. The total length of this circuit is 134 m.

**Table 3.** Activity Rn measured with ERM for the Tests.

Test-1	Test-2	Test-3—I	Test-3—II
$\leq 1.3 \text{ mBq/m}^3$	$\leq 4.3 \text{ mBq/m}^3$	$45.0 \text{ mBq/m}^3$	$31.0 \text{ mBq/m}^3$

Two levels of flow at the entrance of the Castle were used in **Test-3**. **Test-3-I** (conditions similar as in Test-1 and Test-2), was performed with a flow of  $\sim 400 \text{ L/m}$ . For **Test-3-II**, a larger flow of  $\sim 550 \text{ L/min}$  was (see Figure 16) used. The Rn-free air significantly reduces the amount of radon (factor larger than 1000) in the neighborhood of the NEXT-100 vessel, a number that varies with the air flow.

Before the ATEKO-air diffusor installation was completed, a study of the influence of the Rn concentration outside the detector (between  $60$  and  $100 \text{ Bq/m}^3$  - measured with an AlphaGuard detector) on NEXT background was performed with the NEXT-White detector (see Figure 17) [17]. A linear correlation may be used to estimate the background rate in NEXT detector and the Rn concentration outside the vessel. Extrapolating the red dashed line to a Rn-free scenario, the expected background rate was  $3.97 \pm 0.46 \text{ mHz}$ . During the background run of NEXT-White, data has been taken first without ATEKO-air (run IVa) and later with ATEKO-air flowing around the detector (run IVb). Without ATEKO-air, the background rate was  $8.00 \pm 0.05 \text{ (stat)} \pm 0.07 \text{ (sys)} \text{ mHz}$ , and with ATEKO-air was  $3.90 \pm 0.05 \text{ (stat)} \pm 0.04 \text{ (sys)} \text{ mHz}$  (see Figure 18) [17]. The result of run IVb and the previous extrapolation are in a very good agreement. In Run IVc an additionally second inner lead shield was mounted. In this run the background rate was reduced to  $2.78 \pm 0.03 \text{ (stat)} \pm 0.03 \text{ (sys)} \text{ mHz}$ .

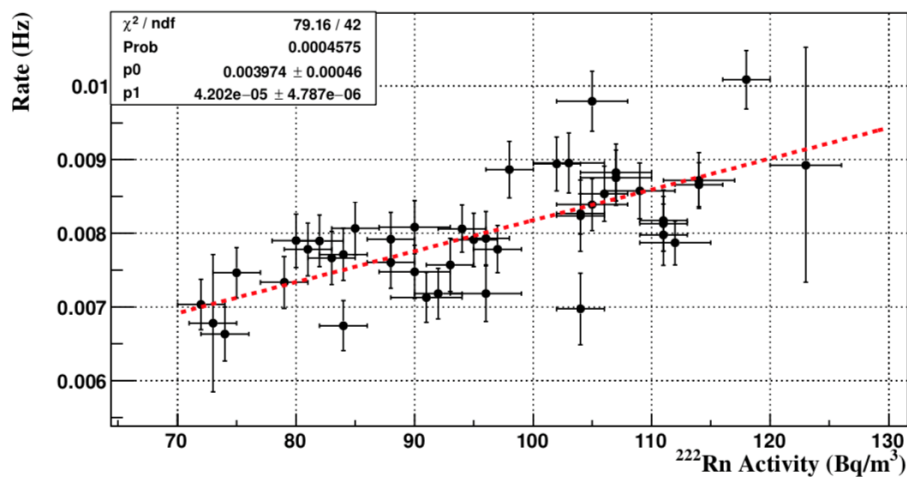


**Figure 17.** Daily Radon activity vs. Background rate in NEXT-White [17].

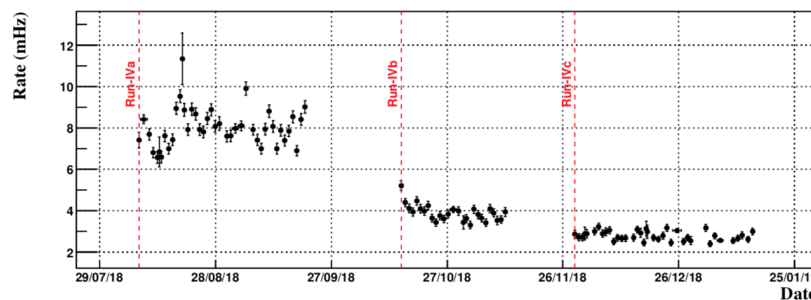


**Figure 18.** Evolution of the total background in NEXT-White detector. The vertical dashed red lines indicate the beginning of each run [17].

## 6. ATEKO-Air to ULBS

The Ultra-Low Background Service (ULBS), working since 2010 in Hall C of LSC (Figure 19), is offering a high-quality screening facility to experiments [4]. At present, it is equipped with six 2 kg p-type coaxial High Purity Germanium (HPGe) detectors with  $\sim 100\%$  relative efficiency, shielded with 20 cm of lead with a low contamination in  $^{210}\text{Pb}$  ( $< 30$  mBq/kg). An internal 10 cm of OFHC (Oxygen-Free High thermal Conductivity) copper layer completes the shielding. The ULBS carries out mainly radio-purity assay for experiments running at LSC and collaborations [18–21] and also contributes to SK-Gd [22] and HK [23] experiments in Kamioka.



Figure 19. ULBS laboratory in Hall C of LSC.

Long measurements (about 30 days) are necessary to reach sensitivity levels of 1 mBq/kg or less, with the condition that the Radon contained in the air inside the HPGe-detector shielding is at the level of 1 mBq/m<sup>3</sup> or less. For this purpose, each detector has an extra layer of shielding made of methacrylate that externally surrounds the lead shielding. To impede the exterior air (and the Rn) from entering inside the shielding, a slight overpressure is created inside the copper shielding. The inner volume available for sample measurement (the inside of the Cu shielding) has the geometry of a cube with side 350 mm (see Figure 20). This gives a volume of  $\sim 43$  L.

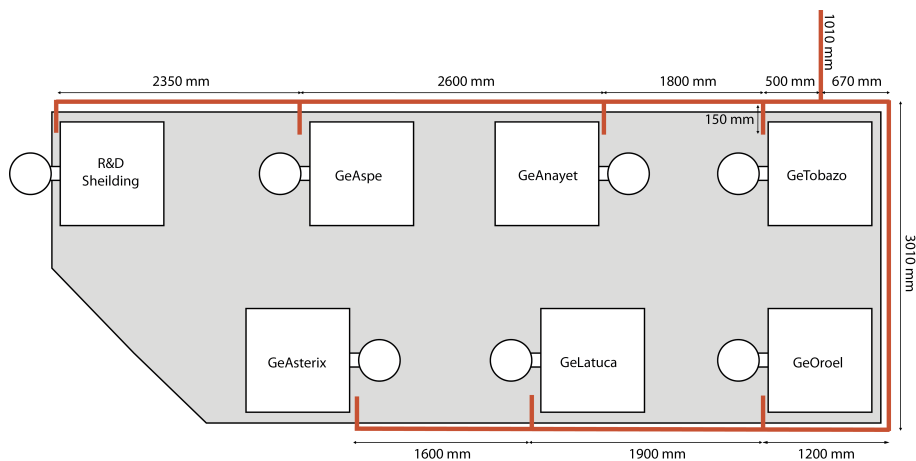


Figure 20. Sample volume inside the Cu shielding.

Two systems are used to reduce the Rn concentration inside the HPGe-detector copper shielding. The first system uses the nitrogen that is evaporating from the detector's dewar. Each HPGe-detector in LSC is equipped with a 30 L dewar for LN<sub>2</sub> necessary for the detector operation. LN<sub>2</sub> has to be refilled each week. Using a 6 mm diameter Teflon tube,

we flush continuously  $\sim 54$  L/h inside the detector the  $N_2$  gas which is evaporating from the dewar. This value was obtained by measuring (with a graded stick) the height of  $LN_2$  and calculate the evaporated gas considering that each liter of  $LN_2$  will produce  $\sim 696$  L of gaseous  $N_2$ . Before the RAS, this setup was the only anti-Radon system.

The second system, using the RAS, reduces even more the total background of the HPGe detectors. A fixed installation was specially built in 2019 to flow ATEKO-air inside the shielding of the detectors (Figure 21). We did some tests and we concluded that there is no difference in the detector’s background rate when using the  $LN_2$  evaporation or ATEKO-air if the flow inside the shielding has the same value. Currently, the flow is 220 L/h in each detector. This flow rate can be regulated with a valve for each detector and the flux is measured with a rotameter (see Figures 22 and 23).



**Figure 21.** Schematic of HPGe positioning in Hall C. In red, the installation to supply ATEKO-Air to each detector.



**Figure 22.** ATEKO-Air main line in Hall C.



**Figure 23.** ATEKO-Air Rotameter with valve to measure and regulate air flow rate.

To optimize the use of the ATEKO-air and obtain a proper Radon reduction we are using both systems. The total flux (ATEKO-air + N<sub>2</sub>) flushed inside the detector is ~274 L/h so the air is changed more than 6 times per hour in the sample volume.

To show the background reduction, we compare (Table 4 and Figure 24) the rates of GeOroel (one of the best HPGe’s of LSC) with the old (2016) and the current setup, i.e., N<sub>2</sub> evaporated from the dewar versus ATEKO-air injected and N<sub>2</sub> evaporated from the dewar.

**Table 4.** Background counts in the 2 setups: 2016-setup with a flux of N<sub>2</sub> from dewar evaporation of 54 L/h; 2021-setup with a flux of 274 L/h made by combined N<sub>2</sub> from dewar evaporation and ATEKO-Air.

	Flux [L/h]	Gas	Int. Rate [40–2700 keV] [cts/kg/day]	Int. Rate [609.32 keV Peak] [cts/kg/day]
2016 setup	54	N <sub>2</sub>	165.3	2.9
2021 setup	274	N <sub>2</sub> +Air	141.8	0.4

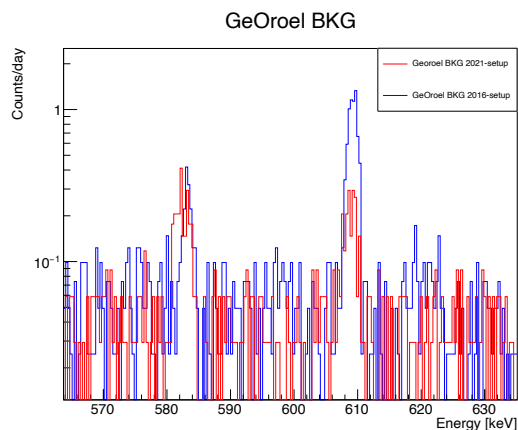


**Figure 24.** GeOroel background comparison, <sup>214</sup>Bi 609.32 keV peak of reduction. In blue 2016 setup vs. in red 2021-setup.



### 7. ATEKO-Air to CROSS Experiment

The goal of the Cryogenic Rare-event Observatory with Surface Sensitivity (CROSS) [24–26] is the development of a technology capable of investigating lepton number violation and the nature of neutrino with unprecedented sensitivity, by searching for neutrinoless double beta decay  $0\nu\beta\beta$  of two promising isotopes ( $^{100}\text{Mo}$  and  $^{130}\text{Te}$ ) with the bolometric approach. The choices of the candidates and of the compounds for CROSS are based on years of development of the bolometric search for  $0\nu\beta\beta$  decay projects: MI-BETA, Cuoricino, CUORE, LUCIFER, CUPID-0, LUMINEU and CUPID-Mo (see [24] and bibliography inside). The baseline solution is background reduction by the scintillating-bolometer technology, as proposed in the CUPID project [27,28]. CROSS can provide an adequate background abatement with a major simplification of the detector structure and of the readout.

A dilution refrigerator with an experimental volume of about  $\sim 150$  L was installed in April 2019 in the LSC in the framework of the CROSS project. The CROSS key idea is to provide the bolometric detection technique, ideally tailored to the study of this rare nuclear transition as it features high energy resolution, large efficiency and wide flexibility in the detector material choice—with an additional decisive characteristic: an effective pulse-shape-discrimination (PSD) capability, enabling the rejection of events from surface radioactive impurities and other background-inducing phenomena. CROSS is planning to install a first demonstrator of the CROSS technology in this cryogenic set-up [24]. It will consist of 32  $\text{Li}_2\text{MoO}_4$  crystals grown with molybdenum enriched in  $^{100}\text{Mo}$  at  $>95\%$  level with CROSS technology [25]. The region of interest (ROI) is around 3034 keV. Each crystal is a cube with 45 mm side, for a mass of 0.28 kg. This new detector will pave the way to bolometric experiments with low background levels (see Table 5 [24]) to make possible future large searches penetrating in prospects the normal hierarchy of the neutrino masses.

**Table 5.** Sensitivity of the CROSS demonstrator to be operated in the cryogenic facility of the Canfranc underground laboratory, under two different hypotheses of background level. The efficiency is 75%, compatible with the crystal size of each element. The interval of limits on the effective Majorana neutrino mass  $m_{\beta\beta}$  accounts for a recent compilation of nuclear-matrix-element calculations [24].

Background Level [counts/(keV kg y)]	Live Time [y]	Background Counts in ROI	Feldman-Cousins Count Limit (90% C.L.)	Half-Life Limit [y] (90% C.L.)	$m_{\beta\beta}$ Limits [meV] (90% C.L.)
$10^{-2}$	2	1.40	3.6	$8.5 \times 10^{24}$	124–222
$10^{-3}$	2	0.14	2.5	$1.2 \times 10^{25}$	103–185
$10^{-2}$	5	3.60	4.6	$1.7 \times 10^{25}$	88–159
$10^{-3}$	5	0.36	2.7	$2.8 \times 10^{25}$	68–122

To reach such low levels of background all external contributions must be mitigated. One of these background sources [24] is the Rn in the air outside the experiment ( $69.0 \pm 0.3$ ) Bq/m<sup>3</sup> as we shown above. To remove this background, the system is similar to the one used in the HPGe detectors: an extra tight shielding made of stainless steel was constructed to surround the detector’s cylindrical lead shielding. ATEKO-air is inserted inside this last layer to create a slight overpressure and impede the external air that contains Radon to enter and produce background.

The shielding design is a cylinder made of a 1 mm Stainless Steel sheet with internal diameter  $D = 990$  mm and 1200 mm high (see Figure 25). The shield is made of several components that can be easily assembled. Silicone gaskets and PTFE are used to maintain the ensemble tight. As the free volume that remains inside this anti-Radon shield is relatively small ( $\sim 45$  L), a flux of 280 L/h of ATEKO-air is sufficient to remove the Rn background to the order of 1 mBq/m<sup>3</sup>. The ATEKO-air installation is very similar to that installed in ULBS (Hall C), a Rotameter with a valve will be used to regulate the Rn-free air flux inside the detector. The shield was mounted in the fall 2021 and will be tested in the following CROSS run starting in December 2021.



**Figure 25.** CROSS Anti-Radon Shield.

## 8. Current Plans

The Rn-free air line became a much needed service at the underground lab and will be further exploited in the near future, with new science and technology projects.

NEXT-100, an upgraded version of NEXT-White, consists of a larger vessel TPC filled with 100 kg of  $^{136}\text{Xe}$ -enriched Xe at 15 bar. Some improvements to the NEXT Castle and the corresponding ATEKO-air input system are in progress: remove the painting to reduce radioactive background and improve air sealing. Also, because a larger TPC will be mounted (lower volume of air inside the Castle) we can expect an important reduction of the radioactive background.

The Radon-free air supply is also essential for the Copper Electroforming Services (CES) [29] recently installed in the LSC Clean Room. A major program of improving the service was done recently to obtain the highest radiopurity of the copper produced in Canfranc, currently tested with components for DAMIC experiment [30], and for additive printing. In the near future, it is planned to test the Radon-free air as an inert gas inside the electrolytic bath instead of nitrogen gas.

The Rn-free air from RAS is necessary in the LSC microbiology and molecular biology laboratory. Currently, five experiments have been approved to start their works underground. These experiments are focused on studies of phenotypic and molecular adaptations of biological models, such as microorganisms or small multicellular eukaryotic organisms in low radiation background environment. The RAS will be used to minimize the Rn environmental background, as done in the physics experiments, to fully monitor the background conditions in the experiments.

## 9. Conclusions

The combination of Underground Laboratories and Radon Abatement Systems guarantees an ideal space to study very low background physics. The LSC, with the addition of this RAS, can offer 5 orders of magnitude of cosmic rays suppression and about  $1 \text{ mBq/m}^3$  of  $^{222}\text{Rn}$  activity in air.

This reduction has been demonstrated in several types of detectors. In particular, thanks to a dedicated pipe able to deliver Rn-free air, NEXT-NEW experiment has reduced the contribution of radon to its background budget from 50% to a negligible level. For HPGe detectors, the addition of ATEKO-air to the air flow around the detector has significantly reduced the number of counts in the peaks in the lower part of the  $^{238}\text{U}$  chain.

The use of RAS in the underground lab is continuously growing and will be essential in the coming months and years to further improve the radioactive background environment of experiments and technologies, particularly in the growing activities in biology, where air can not be replaced by nitrogen.

**Author Contributions:** G.Z., K.P., A.W.-P., J.P.-P. contributed to the design and setting-up of ERM; A.B., J.P.-P., J.M.C.-M., S.B.-S. contributed to the setup and maintenance of RAS; P.N., M.S., A.O.d.S., J.T., A.U., B.R., J.P.-P., C.P.-G. contributed to the tests of ATEKO-Air to NEXT; I.C.B., B.H.-M. contributed to HPGe shielding design and maintenance; A.O.d.S., J.M.C.-M. contributed to the design and mounting of CROSS anti-Rn shield; J.C.A., S.B.-S., L.C.-B. design, mounting and measurements of

copper electroforming; R.H.-A. mounting of the biology experiments; C.P.-G. facility operation; I.C.B. radon measurements. All authors have read and agreed to the published version of the manuscript.

**Funding:** This research was funded in part by the European Regional Development Fund (ERDF), corresponding to the 2013–2016 Spanish Scientific and Innovation Research Program, grants No. CPEE15-EE-3829 and No. CPEE13-4E-2646. This research was supported in part by the Polish National Science Centre (NCN), grant No. UMO-2020/37/B/ST2/03905 and the Polish Ministry of Education and Science grant No. DIR/WK/2018/08. Laboratorio Subterráneo de Canfranc (LSC) is a Spanish Unique Science and Technology Public Research Institution (ICTS) granted by the Spanish Ministry of Science and Innovation, The Regional Government of Aragon and the University of Zaragoza.

**Institutional Review Board Statement:** Not applicable.

**Informed Consent Statement:** Not applicable.

**Data Availability Statement:** Data are available upon request.

**Acknowledgments:** Authors would like to acknowledge the special support from Alfredo Gimeno from LSC in the construction and mounting of the anti-Rn shields and Victor Gimenez for the maintenance of RAS.

**Conflicts of Interest:** The authors declare no conflict of interest. The founding sponsors had no role in the design of the study, collection, analysis or interpretation of data, writing of the manuscript or decision to publish.

## References

- Bettini, A. New underground laboratories: Europe, Asia and the Americas. *Phys. Dark Universe* **2014**, *4*, 36–40. [CrossRef]
- Wójcik, M.; Zuzel, G.; Simgen, H. Review of high-sensitivity Radon studies. *Int. J. Mod. Phys. A* **2017**, *32*, 1743004. [CrossRef]
- LSC Website. Available online: [https://lsc-canfranc.es/wp-content/uploads/2019/03/2017\\_EN.pdf](https://lsc-canfranc.es/wp-content/uploads/2019/03/2017_EN.pdf) (accessed on 20 January 2022).
- Bandac, I.; Borjabad, S.; Ianni, A.; Nunez-Lagos, R.; Perez, C.; Rodriguez, S.; Villar, J.A. Ultra-low background and environmental measurements at Laboratorio Subterráneo de Canfranc (LSC). *Appl. Radiat. Isot.* **2017**, *126*, 127–129. [CrossRef] [PubMed]
- Arvela, H.; Holmgren, O.; Hänninen, P. Effect of soil moisture on seasonal variation in indoor radon concentration: Modelling and measurements in 362 Finnish houses. *Radiat. Prot. Dosim.* **2016**, *168*, 277–290. [CrossRef]
- Shweikani, R.; Giaddui, T.G.; Durrani, S.A. The effect of soil parameters on the radon concentration values in the environment. *Radiat. Meas.* **1995**, *25*, 581–584. [CrossRef]
- Maeng, Y.; Busenitz, J.; Piepke, A. A new method for evaluating the effectiveness of plastic packaging against radon penetration. *Appl. Radiat. Isot.* **2020**, *156*, 108963. [CrossRef]
- Mamedov, F.; Čermák, P.; Smolek, K.; Štekl, I. Measurement of radon diffusion through shielding foils for the SuperNEMO experiment. *J. Instrum.* **2011**, *6*, C01068. [CrossRef]
- Bandac, I.; Bettini, A.; Borjabad, S.; Núñez-Lagos, R.; Pérez, C.; Rodríguez, S.; Sánchez, P.; Villar, J.A. Radón y radiación ambiental en el Laboratorio Subterráneo de Canfranc (LSC). *Radioprotección (SEPR)* **2014**, *XXI*, 24–29.
- Pelczar, K.; Zuzel, G.; Wójcik, M.; Pocar, A.; Ianni, A. An online radon monitor for low-background detector assembly facilities. *Eur. Phys. J. C* **2021**, *81*, 1–12. [CrossRef]
- Hodák, R.; Perrot, F.; Brudanin, V.; Busto, J.; Havelcová, M.; Hůlka, J.; Jullian, S.; Kochetov, O.; Lalanne, D.; Loaiza, P.; et al. Characterization and long-term performance of Radon Trapping Facility operating at the Modane Underground Laboratory. *J. Phys. G Nucl. Part. Phys.* **2019**, *46*, 115105. [CrossRef]
- Lee, M.H. Radioassay and Purification for Experiments at Y2L and Yemilab in Korea. *J. Phys. Conf. Ser.* **2020**, *1468*, 012249. [CrossRef]
- ATEKO a.s. Website. Available online: [https://www.ateko.cz/media/cache/file/25/ATEKO\\_Radon\\_Removal\\_Systems\\_2020.pdf](https://www.ateko.cz/media/cache/file/25/ATEKO_Radon_Removal_Systems_2020.pdf) (accessed on 26 January 2022).
- Monrabal, F.; Gómez-Cadenas, J.J.; Toledo, J.F.; Laing, A.; Álvarez, V.; Benlloch-Rodríguez, J.M.; Cárcel, S.; Carrión, J.V.; Esteve, R.; Felkai, R.; et al. (NEXT Collaboration) The Next White (NEW) Detector. *J. Instrum.* **2018**, *13*, P12010. [CrossRef]
- Martín-Albo, J.; Muñoz Vidal, J.; Ferrario, P.; Nebot-Guillot, M.; Gómez-Cadenas, J.J.; Álvarez, V.; Azevedo, C.D.R.; Borges, F.I.G.; Cárcel, S.; Carrión, J.V.; et al. (NEXT Collaboration) Sensitivity of NEXT-100 to neutrinoless double beta decay. *J. High Energ. Phys.* **2016**, *2016*, 1–30. [CrossRef]
- Cebrián, S.; Pérez, J.; Bandac, I.; Labarga, L.; Álvarez, V.; Barrado, A.I.; Bettini, A.; Borges, F.I.; Camargo, M.; Cárcel, S.; et al. Radon and material radiopurity assessment for the NEXT double beta decay experiment. *Aip Conf. Proc.* **2015**, *1672*, 060002.
- Novella, P.; Palmeiro, B.; Sorel, M.; Usón, A.; Ferrario, P.; Gómez-Cadenas, J.J.; Adams, C.; Álvarez, V.; Arazi, L.; Arnquist, I.J.; et al. Radiogenic backgrounds in the NEXT double beta decay experiment. *J. High Energy Phys.* **2019**, *2019*, 1–26.

18. Cebrián, S.; Pérez, J.; Bandac, I.; Labarga, L.; Álvarez, V.; Azevedo, C.D.R.; Benlloch-Rodríguez, J.M.; Borges, F.I.G.M.; Botas, A.; Cárcel, S.; et al. Radiopurity assessment of the energy readout for the NEXT double beta decay experiment. *J. Instrum.* **2017**, *12*, T08003. [[CrossRef](#)]
19. Dafni, T.; Álvarez, V.; Bandac, I.; Bettini, A.; Borges, F.I.; Camargo, M.; Cárcel, S.; Cebrián, S.; Cervera, A.; Conde, C.A.; et al. Results of the material screening program of the NEXT experiment. *Nucl. Part. Phys. Proc.* **2016**, *273*, 2666–2668. [[CrossRef](#)]
20. Tzika, F.; Hult, M.; Fenyvesi, A.; Bandac, I.; Degering, D.; Ianni, A.; Laubenstein, M.; de Vismes-Ott, A.; Marissens, G.; Stroh, H.; et al. Coordinate underground measurements of gamma-ray emitting radionuclides for plasma physics research. *Appl. Radiat. Isot.* **2017**, *126*, 121–126. [[CrossRef](#)]
21. Picado, E.; Fraile, L.M.; Bandac, I.; Udias, J.M. Radiopurity Study of an Encapsulated CeBr<sub>3</sub> crystal. *JPS Conf. Proc.* **2015**, *6*, 030133.
22. Marti, L.; Ikeda, M.; Kato, Y.; Kishimoto, Y.; Nakahata, M.; Nakajima, Y.; Nakano, Y.; Nakayama, S.; Okajima, Y.; Orii, A.; et al. Evaluation of gadolinium's action on water Cherenkov detector systems with EGADS. *Nucl. Instrum. Methods A* **2020**, *959*, 163549 [[CrossRef](#)]
23. Abe, K.; Abe, K.; Aihara, H.; Aimi, A.; Akutsu, R.; Andreopoulos, C.; Anghel, I.; Anthony, L.H.V.; Antonova, M.; Ashida, Y.; et al. Hyper-Kamiokande Design Report. *arXiv* **2018**, arXiv:1805.04163
24. Bandac, I.C.; Barabash, A.S.; Bergé, L.; Brière, M.; Bourgeois, C.; Carniti, P.; Chapellier, M.; de Combarieu, M.; Dafinei, I.; Danevich, F.A.; et al. (CROSS Collaboration) The  $0\nu 2\beta$ -decay CROSS experiment: Preliminary results and prospects. *J. High Energ. Phys.* **2020**, *2020*, 1–31. [[CrossRef](#)]
25. Bandac, I.C.; Barabash, A.S.; Bergé, L.; Bourgeois, C.; Calvo-Mozota, J.M.; Carniti, P.; Chapellier, M.; deCombarieu, M.; Dafinei, I.; Danevich, F.A.; et al. (CROSS Collaboration) Phonon-mediated crystal detectors with metallic film coating capable of rejecting  $\alpha$  and  $\beta$  events induced by surface radioactivity. *Appl. Phys. Lett.* **2021**, *118*, 184105. [[CrossRef](#)]
26. Armatol, A.; Armengaud, E.; Armstrong, W.; Augier, C.; Avignone III, F.T.; Azzolini, O.; Bandac, I.C.; Barabash, A.S.; Bari, G.; Barresi, A.; et al. (CROSS Collaboration) A CUPID Li<sub>2</sub> <sup>100</sup>MoO<sub>4</sub> scintillating bolometer tested in the CROSS underground facility. *J. Instrum.* **2021**, *16*, P02037. [[CrossRef](#)]
27. CUPID Collaboration. CUPID pre-CDR. *arXiv* **2019**, arXiv:1907.09376.
28. CUPID Collaboration. CUORE (Cryogenic Underground Observatory for Rare Events) Upgrade with Particle IDentification. *arXiv* **2015**, arXiv:1504.03599.
29. Borjabad, S.; Amaré, J.C.; Bandac, I.C.; di Vacri, M.L.; Ianni, A.; Nisi, S. Copper electroforming service at Laboratorio Subterráneo de Canfranc (LSC). *AIP Conf. Proc.* **2018**, *1921*, 020001.
30. DAMIC-M Website. Available online: <https://damic.uchicago.edu/> (accessed on 25 January 2022).